

Submitted to Z. Phys. B0

Magnetic and Dynamic Properties of the Hubbard Model in Infinite Dimensions

Mark Jarrell

Department of Physics

University of Cincinnati

Cincinnati, Ohio 45221

and

Thomas Pruschke

Department of Physics

The Ohio State University

Columbus, Ohio 43210

May, 1992

Abstract

An essentially exact solution of the infinite dimensional Hubbard model is made possible by using a self-consistent mapping of the Hubbard model in this limit to an effective single impurity Anderson model. Solving the latter with quantum Monte Carlo procedures enables us to obtain exact results for the one and two-particle properties of the infinite dimensional Hubbard model. In particular we find antiferromagnetism and a pseudogap in the single-particle density of states for sufficiently large values of the intrasite Coulomb interaction at half filling. Both the antiferromagnetic phase and the insulating phase above the Néel temperature are found to be quickly suppressed on doping. The latter is replaced by a heavy electron metal with a quasiparticle mass strongly dependent on doping as soon as $n < 1$. At half filling the antiferromagnetic phase boundary agrees surprisingly well in shape and order of magnitude with results for the three dimensional Hubbard model.

PACS numbers: 71.10+x, 75.10.Jm, 75.10.Lp, 75.30.Kz.

1 Introduction

The Hubbard model [1] of strongly correlated electron systems has been an enduring problem in condensed matter physics. It is believed to at least qualitatively describe some of the properties of transition metal oxides, and possibly high temperature superconductors [2]. Using standard notation, the Hubbard Hamiltonian reads [1]

$$\begin{aligned} \mathcal{H} = & -t \sum_{\langle ij \rangle, \sigma} (C_{i,\sigma}^\dagger C_{j,\sigma} + C_{j,\sigma}^\dagger C_{i,\sigma}) \\ & + \sum_i [\epsilon (n_{i,\uparrow} + n_{i,\downarrow}) + U (n_{i,\uparrow} - 1/2) (n_{i,\downarrow} - 1/2)] \end{aligned} \quad (1)$$

where $C_{i,\sigma}$ ($C_{i,\sigma}^\dagger$) destroys (creates) an electron of spin σ on site i of a hypercubic lattice of dimension d , and $n_{i,\sigma} = C_{i,\sigma}^\dagger C_{i,\sigma}$. Despite the simplicity of the model, no exact solutions exist except in one dimension, where the knowledge is in fact rather complete [3]. The unusual properties in one dimension also gave rise to discussions of whether the behaviour in 2D could be related to the 1D case [4]. The extent that this very special limit can serve as a reference point for any finite dimensional model [5, 6] remains controversial, and an examination of the model from a different point of view is clearly needed.

Recently, a new approach [7, 8, 9] based on an expansion in $1/d$ about the point $d = \infty$ has been proposed to study such strongly correlated lattice models. In this limit the requirement of a finite total energy per site makes

it necessary to rescale nonlocal interactions by an appropriate power of d^{-1} [7, 8]. While e.g. spin-exchange will essentially reduce to the corresponding mean field theory results [8], interactions like the screened Coulomb repulsion in the model (1) remain nontrivial even in this limit.

In a previous short paper [10], one of us presented the first method of exact solution of the Hubbard model in the infinite dimensional limit. In this paper, we provide a greatly expanded discussion of the method and the physics. The model in the infinite dimensional limit retains the physics expected in the low dimensional model, e.g. antiferromagnetism and the formation of a correlation induced Mott-Hubbard pseudogap in the single-particle density of states. In addition, we find some very interesting structures in the single-particle density of states (DOS), which we believe will persist in $d < \infty$ and lead to well defined and observable effects, which may serve as a guide whether the model is indeed capable of describing the essentials of transition metal physics.

2 Theory and Numerical Considerations

The limit as $d \rightarrow \infty$ is taken such that $4t^2d = t^{*2} = \text{constant}$ and it is convenient to choose $t^* = 1$ as the energy scale for the remainder of this paper. This rescaling of the kinetic energy automatically leads to a finite net effective magnetic exchange $dJ \sim t^{*2}/U$. Generally this limit provides two

large simplifications. First, the free DOS for near-neighbor transfer along the coordinate axis can be shown to acquire a Gaussian form, i.e. [7, 8]

$$\rho_0(t) = \exp(-t^2)/\sqrt{\pi} . \quad (2)$$

Second, the problem reduces essentially to a local one since nonlocal dynamical interactions become negligible in this limit [7, 8]. For example, the irreducible self energy and the irreducible vertex functions purely are local.

This may be seen from a diagrammatic argument [11]. Consider the first few diagrams of the single-particle self-energy for this problem as shown in Fig. 1. This is a real-space representation, so each electron propagator G_{ij}

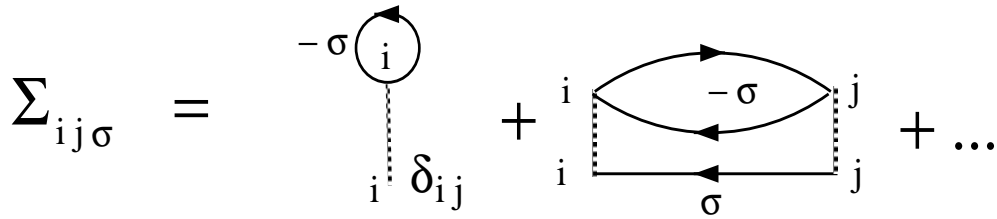


Figure 1: *First few diagrams for the lattice self energy. Here, the solid lines represent the undressed ($U = 0$) electron propagators $G_{ij}^0(i\omega_n)$, and the dashed lines represent the local Coulomb interaction U .*

scales as $\sim t^{-|\mathbf{R}_i - \mathbf{R}_j|}$. Thus the second order term in Fig. 1 scales as $t^{-3|\mathbf{R}_i - \mathbf{R}_j|}$ and, after summing over the contribution of the nearest neighbor shell, gives a contribution of the order $d \cdot d^{-3/2}$ (since $4t^2d = 1$). This contribution vanishes in the limit as $d \rightarrow \infty$. A similar argument may be applied to all terms, and

only the site diagonal self-energy survives the limit $d \rightarrow \infty$. Furthermore, since the lattice is translationally invariant $\Sigma_{ij}(i\omega_n) = \Sigma(i\omega_n)\delta_{ij}$ independent of i . Thus, Dyson's equation reduces to

$$G_{ij}(i\omega_n) = G_{ij}^0(i\omega_n) + \sum_k G_{ik}^0(i\omega_n)\Sigma(i\omega_n)G_{kj}(i\omega_n) \quad (3)$$

with the diagrammatic equation for $\Sigma(z)$ in Fig. 1. A completely equivalent argument may be used for the magnetic susceptibility [12], which reads

$$\begin{aligned} \chi_{ij}(i\nu_n) &= \frac{1}{\beta} \sum_{\omega_n, \omega_m} \tilde{\chi}_{ij}(i\omega_n, i\omega_m; i\nu_n) \\ \tilde{\chi}_{ij}(i\omega_n, i\omega_m; i\nu_n) &= \tilde{\chi}_{ij}^0(i\omega_n; i\nu_n)\delta_{nm} \\ &\quad + \frac{1}{\beta} \sum_{\omega_p, l} \tilde{\chi}_{il}^0(i\omega_n; i\nu_n)\Gamma(i\omega_n, i\omega_p; i\nu_n)\tilde{\chi}_{lj}(i\omega_p, i\omega_m; i\nu_n) \\ \tilde{\chi}_{ij}^0(i\omega_n; i\nu_n) &= \frac{1}{N^2} \sum_{\mathbf{k}, \mathbf{q}} e^{i\mathbf{q}\cdot(\mathbf{R}_i - \mathbf{R}_j)} G_{\mathbf{k}}(i\omega_n)G_{\mathbf{k}+\mathbf{q}}(i\omega_n + i\nu_n) \end{aligned} \quad (4)$$

where $\beta = (k_B T)^{-1}$, ω_n (ν_n) are the Fermi- (Bose-) Matsubara frequencies, $G_{\mathbf{k}}(z)$ is the one particle Green's function obtained from (3) and $\Gamma(z, z')$ the irreducible vertex.

Usually, quantities like the self-energy $\Sigma(z)$ and $\Gamma(z, z')$ have to be evaluated using a direct perturbation expansion as outlined in Fig. 1. With respect to U this has been done for the present model quite extensively by means of conserving approximations including particle-hole and particle-particle ladder summations [13]. Alternatively, one of us recently proposed a perturba-

tion theory using the transfer term t as expansion parameter [14]. However, as one knows from similar studies for heavy fermion systems, the validity and radius of convergence of these expansions may depend critically on the particular choice of parameters [15]. In the following we therefore want to present an approach which maps the whole problem to the solution a single impurity Anderson model, where several reliable ways to obtain the solution are known. That this connection exists was realized quite early [16], but until now it only served to set up equations for the thermodynamic potential [16, 17].

To do this let us return to equation (3). For $i = j$, the diagrams contributing to the local Green's function $\mathcal{G} \equiv G_{ii}$ may be rearranged to contain explicitly only local processes as illustrated in Fig. 2. The undressed Green's

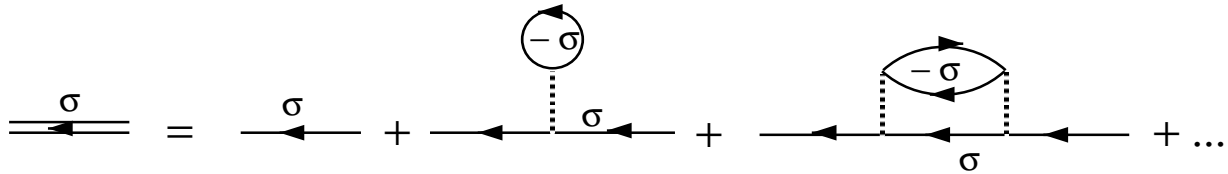


Figure 2: *First few diagrams for the local Green's function \mathcal{G} (double solid line). The diagrams have been rearranged such that all processes occurring on other sites than the one considered were included into an effective host Green's function $\tilde{\mathcal{G}}$ represented here as a solid line. The Coulomb interacting is again visualized as a dashed line.*

function represented by the solid line in Fig. 2 must incorporate the missing nonlocal processes and thus is the solution to a modified lattice problem

$$\tilde{\mathcal{G}}(i\omega_n) = \tilde{G}_{ii}(i\omega_n) = G_{ii}^0(i\omega_n) + \sum_k' G_{ik}^0(i\omega_n) \Sigma(i\omega_n) \tilde{G}_{ki}(i\omega_n) \quad (5)$$

where the prime at the sum indicates that $k \neq i$ and $G_{ij}^0(z)$ is the unperturbed propagator. This summation restriction is necessary to avoid over-counting of local diagrams. In reciprocal space, equation (5) reads

$$\tilde{G}_{\mathbf{k}}(i\omega_n) = G_{\mathbf{k}}^0(i\omega_n) + G_{\mathbf{k}}^0(i\omega_n) \Sigma(i\omega_n) \left(\tilde{G}_{\mathbf{k}}(i\omega_n) - \tilde{\mathcal{G}}(i\omega_n) \right) . \quad (6)$$

This may be solved for $\tilde{G}_{\mathbf{k}}(z)$ and summed on \mathbf{k} to yield

$$\frac{1}{\tilde{\mathcal{G}}(z)} = \frac{1}{\mathcal{G}(z)} + \Sigma(z) . \quad (7)$$

The problem closes by noting two things. First, Fig. 2 is nothing but the perturbation expansion of an Anderson impurity model with a host Green's function specified by $\tilde{\mathcal{G}}$. In the spirit of this analogy, one may then define an effective hybridization strength $\Delta(z)$ via [18]

$$\Delta(z) = \frac{1}{\tilde{\mathcal{G}}(z)} - z + \epsilon . \quad (8)$$

Secondly, $\Sigma(z)$ and $G_{ii}(z)$ are as usual related by

$$G_{ii}(z) = \int d\omega \rho_0(\omega) \frac{1}{z - \omega - \epsilon - \Sigma(z)} . \quad (9)$$

However, $G_{ii}(z)$ is by definition also the propagator of the effective Anderson impurity problem *defined* by equation (8). Let us emphasize, that, although

we used the formal perturbation expansion of the model (1) in terms of U in our discussion, it does not enter the set of equations (5)-(9) at any stage. This means that we did not refer to any special method to solve the impurity Anderson model and that equations (5)-(9) are exact.

In the present paper we should like to concentrate on the quantum Monte Carlo (QMC) algorithm of Hirsch and Fye [19, 20] as a method to solve the impurity Anderson model, although equivalent calculations were done using a self-consistent perturbation scheme (NCA) for this problem [21]. These calculations generally use considerably less computational time and, away from some critical region at half filling, the results found were in good agreement with the QMC [22]. However, with respect to two-particle properties the QMC is simply the more adequate approach, since the NCA requires the solution of difficult Bethe-Salpeter type equations as soon as finite Coulomb repulsion is considered.

In the QMC the problem is cast into a discrete path formalism in imaginary time, τ_l , where $\tau_l = l\Delta\tau$, $\Delta\tau = \beta/L$, and L is the number of time slices. The values of L used ranged from 40 to 160, with the largest values of L reserved for the largest values of β since the time required by the algorithm increases like L^3 . No sign problem was encountered in the QMC process, except for extremely large values of U away from half filling. Even here, the sign problem was mild, and easily handled with the standard methods. The self-consistency process described above is easily employed in the QMC pro-

cess. Choosing an initial Σ , the output of the process is \mathcal{G} , which may then be inverted to yield a new estimate for $\Sigma(i\omega_n)$ and so on until $\mathcal{G} = G_{ii}$ within the numerical precision. Usually 4–8 iterations are required for convergence. Other quantities such as the unscreened local moment $\mu^2 = \langle (n_\uparrow - n_\downarrow)^2 \rangle$, the two-particle Green's functions equation (4) etc. are calculated on the last iteration, once convergence is reached. Typical systematic (due to finite $\Delta\tau$) and statistical errors were quite small, usually less than 1%. Thus, unless explicitly displayed, the error bars on the static quantities may be assumed to be smaller than the plotting symbols.

3 Two-Particle Properties

As already mentioned, a variety of two-particle properties may be calculated with this procedure. Here we want to concentrate on the antiferromagnetic static susceptibility, given by (4) for $i\nu \rightarrow 0$ at $\mathbf{q} = \mathbf{Q} = (\pi, \pi, \dots)$. Except for the one particle propagators discussed in the next section, the only unknown quantity there is the local vertex Γ . However, because it involves only local processes, it can be determined from the susceptibility of the impurity

Anderson model, which may be obtained from

$$\begin{aligned} \tilde{\chi}_{ii}(i\omega_n, i\omega_m; i\nu_n) = & \tilde{\chi}_{ii}^0(i\omega_n; i\nu_n)\delta_{nm} \\ & + \frac{1}{\beta} \sum_p \tilde{\chi}_{ii}^0(i\omega_n; i\nu_n)\Gamma(i\omega_n, i\omega_p; i\nu_n)\tilde{\chi}_{ii}(i\omega_p, i\omega_m; i\nu_n) \end{aligned} \quad (10)$$

Here $\tilde{\chi}_{ii}$ is the opposite-spin two-particle Green's function matrix,

$$\begin{aligned} \tilde{\chi}_{ii}(i\omega_n, i\omega_m; i\nu_n) = & -\frac{1}{\beta^2} \int_0^\beta d\tau_1 \int_0^\beta d\tau_2 \int_0^\beta d\tau_3 \int_0^\beta d\tau_4 e^{-i\omega_m(\tau_1-\tau_2)} e^{-i\omega_n(\tau_3-\tau_4)} \\ & e^{i\nu_n(\tau_2-\tau_4)} \left\langle T_\tau C_{i,\uparrow}(\tau_4) C_{i,\downarrow}^\dagger(\tau_3) C_{i,\downarrow}(\tau_2) C_{i,\uparrow}^\dagger(\tau_1) \right\rangle. \end{aligned} \quad (11)$$

If we substitute (10) into (4), we obtain for $i\nu \rightarrow 0$ the matrix relation

$$\tilde{\chi}_{\mathbf{q}}^{-1} = \tilde{\chi}_{\mathbf{q}}^{0-1} + \tilde{\chi}_{ii}^{-1} - \tilde{\chi}_{ii}^{0-1} \quad (12)$$

where the static susceptibility is obtained by summing

$$\chi_{\mathbf{q}}(T) = \frac{1}{\beta} \sum_{mn} \tilde{\chi}_{\mathbf{q}}(i\omega_n, i\omega_m) \quad (13)$$

It is expected that the Hubbard model on a cubic lattice with nearest-neighbour transfer will exhibit antiferromagnetism at half filling for arbitrary values of U due to perfect nesting [23]. This transition is signaled by the divergence of the antiferromagnetic susceptibility χ_{AF} calculated using the methods described above. Results from this approach are shown in Fig. 3 for $U = 1.5$ and $\epsilon = 0$. The logarithmic scaling behaviour is shown in the inset. Near the Neél temperature T_N the data fit a form $\chi_{AF} \propto |T - T_N|^\nu$

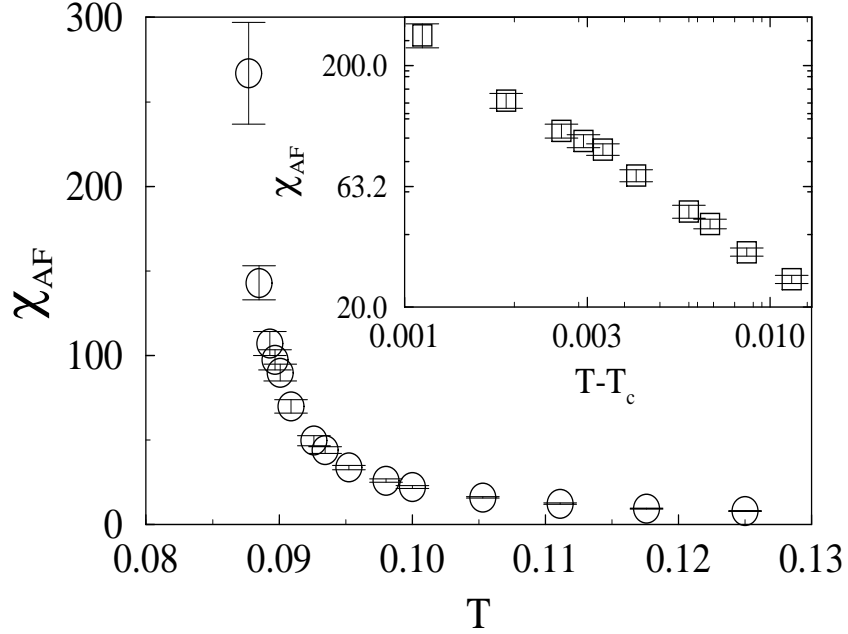


Figure 3: *Antiferromagnetic susceptibility $\chi_{AF}(T)$, versus temperature T when $U = 1.5$ and $\epsilon = 0.0$. The logarithmic scaling behaviour is shown in the inset. The data close to the transition fit the form $\chi_{AF} \propto |T - T_N|^\nu$ with $T_N = 0.0866 \pm 0.0003$ and $\nu = -0.99 \pm 0.05$ consistent with the mean-field behaviour expected for $d = \infty$.*

with $T_N = 0.0866 \pm 0.0003$ and $\nu = -0.99 \pm 0.05$. This scaling behaviour is consistent with that of a Heisenberg model on a lattice with an infinite number of nearest neighbors, for which one expects the Curie-Weiss mean-field form for χ_{AF} .

The antiferromagnetic transition temperature T_N for the half-filled model

obtained within the current approach is plotted as a function of U in Fig. 4a.

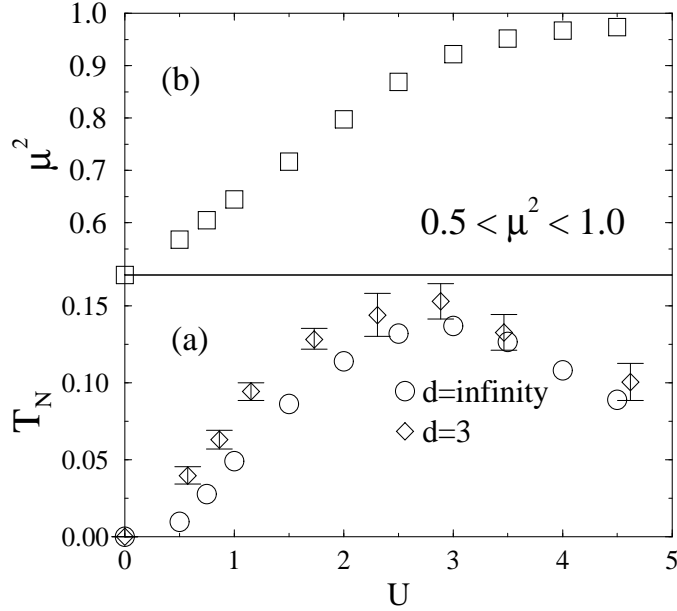


Figure 4: (a) Antiferromagnetic T_N and (b) $\mu^2 = \langle (n_\uparrow - n_\downarrow)^2 \rangle$ (calculated at $T = T_N$) as functions of U for the half-filled model ($\epsilon = 0$). In (a) the circles represent the values obtained from the present approach while the diamonds are data for a three dimensional Hubbard model extracted from ref. 24.

For small values of U , where the local spin moment is also small, we find that T_N is exponentially small, consistent with perturbation theory [24]. For very large values of U , where the spin moment has saturated to its maximum value, one expects that the transition temperature will fall monotonically with increasing U , $T_N \sim 1/U$ [24]. This is because the antiferromagnetic exchange $dJ \sim t^2/U$ also decreases with increasing U . Thus, one expects

a peak in $T_N(U)$ for some intermediate value of U as seen in Fig. 4a. For comparison we included in Fig. 4a also $T_N(U)$ for the $d = 3$ Hubbard model as calculated by Scalettar et al. [25]. The shape and order of magnitude compare very well, although the $d = 3$ data always have slightly larger values, which we think is partially a consequence of the different analytic structures of the free DOS in $d = 3$ and $d = \infty$ [26]. In Fig. 4b the unscreened squared magnetic moment $\mu^2 = \langle (n_\uparrow - n_\downarrow)^2 \rangle$, calculated at the transition $T = T_N$, is plotted versus U when $\epsilon = 0$. For the half-filled model μ^2 ranges from $\mu^2 = 0.5$ in the uncorrelated limit ($U = 0$), to $\mu^2 = 1$ in the strongly

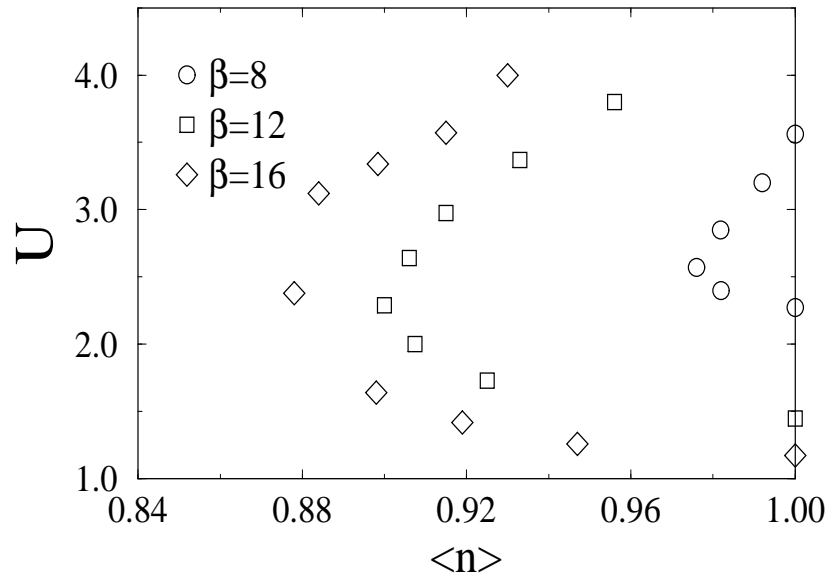


Figure 5: *Critical values of U , where χ_{AF} diverges, versus filling for several temperatures. The result is symmetric around $\langle n \rangle = 1$.*

correlated limit ($U \rightarrow \infty$). Note that the peak in $T_N(U)$ occurs near the point where μ^2 begins to saturate to one. Away from half filling, the divergence of the antiferromagnetic susceptibility is quickly suppressed. This behaviour is shown in Fig. 5 where the critical value of U is plotted versus filling for several values of β .

In contrast to the antiferromagnetic susceptibility, the ferromagnetic susceptibility ($\mathbf{q} = (0, 0, \dots)$) is rather featureless both as a function of temperature and filling. This behaviour is shown in Fig. 6 where χ_F is plotted

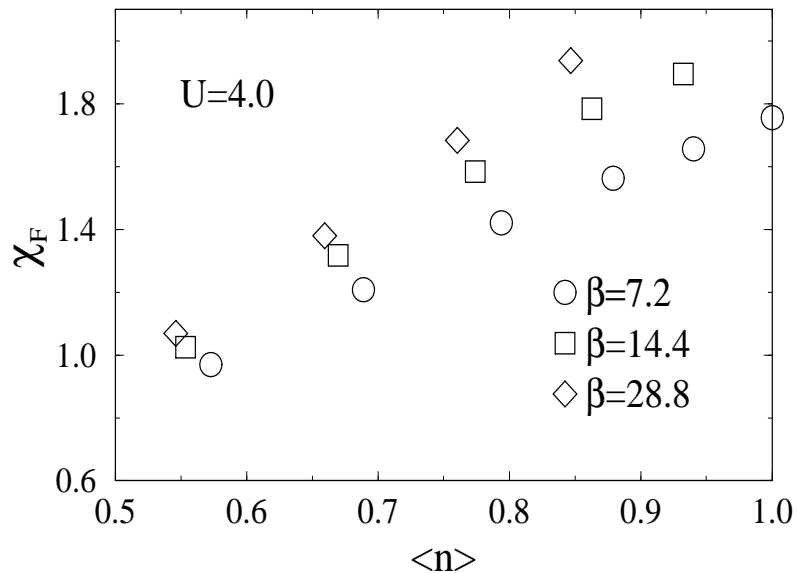


Figure 6: *The χ_F versus filling, when $U = 4$. χ_F was not calculated at half filling when $\beta = 14.4$ and $\beta = 28.8$ since χ_{AF} has already diverged here.*

versus filling for several temperatures when $U = 4$. For values of U as large

as eight, the ferromagnetic susceptibility never diverged. Special attention was placed near the region just off half filling for large U where one might expect Nagaoka behaviour. In this region, for $U = 8$, χ_F did show a mild peak as a function of filling. However, this data was prone to excessive error bars, and in all such cases $\chi_{AF} \gg \chi_F$.

In addition to ferromagnetic and antiferromagnetic behaviour, it is possible that the infinite dimensional Hubbard model may exhibit incommensurate order away from half filling. Such calculations were not included here but are left for future study.

By a method very similar to that used to calculate the magnetic susceptibilities, one may also calculate the superconducting pair-field susceptibilities. Since singlet superconducting order parameters with the same symmetry (eg. s-wave and extended s-wave) mix, the possible divergencies of all pair field susceptibilities with the same symmetry must coincide. Thus, it is only necessary to calculate one susceptibility of each symmetry. Furthermore, in the infinite dimensional limit, a pair-field susceptibility which corresponds to a symmetry orthogonal to the lattice symmetry (extended s-wave symmetry) has no vertex corrections. Consider a superconducting channel which has a form factor $t_{\mathbf{k}}$ such that

$$\sum_{\mathbf{k}} t_{\mathbf{k}} |G(\mathbf{k}, i\omega_n)|^2 = 0 . \quad (14)$$

The first two diagrams in the corresponding pair-field susceptibility are shown

in figure 7. When $d = \infty$ the irreducible vertex has no \mathbf{k} -dependence so the

$$\sum_{\mathbf{n} \mathbf{k}} \begin{array}{c} \xrightarrow{i \omega_{\mathbf{n}} \mathbf{k}} \\ t_{\mathbf{k}} \quad t_{\mathbf{k}} \\ \xleftarrow{-i \omega_{\mathbf{n}} -\mathbf{k}} \end{array} + \sum_{\substack{\mathbf{k}' \mathbf{k} \\ \mathbf{n} \mathbf{m}}} \begin{array}{c} \xrightarrow{i \omega_{\mathbf{m}}} \\ t_{\mathbf{k}'} \quad \Gamma_{\mathbf{S}} \quad t_{\mathbf{k}} \\ \xleftarrow{-i \omega_{\mathbf{m}}} \quad \xleftarrow{-i \omega_{\mathbf{n}}} \end{array} + \dots$$

Figure 7: *First two diagrams for the superconducting pair-field susceptibility. The form factor $t_{\mathbf{k}}$ determines the symmetry of the pairing. If the symmetry of $t_{\mathbf{k}}$ is orthogonal to s-wave, then the vertex corrections vanish.*

sum over \mathbf{k} may be performed independently on the right and left-hand sides of the vertex in the second term. Thus, when $t_{\mathbf{k}}$ is consistent with Eq. 14, this term vanishes. The only diagram which remains is the simple bubble which can only diverge in the zero-temperature limit. This argument may be extended to any superconducting order parameter which is orthogonal to s-wave, leaving only the possibility of superconductivity with s-wave symmetry. However, for all parameters discussed here we found that the s-wave pair-susceptibility remained finite at a value below the non-interacting limit. Thus, we conclude that there is no singlet superconductivity in the infinite dimensional Hubbard model.

4 Single-Particle Properties

In this section we will discuss the single-particle properties of the Hubbard model (1) as $d = \infty$. The most important quantity in this connection is the single particle density of states defined by $A(\omega) = -1/\pi \text{Im}G_{ii}(\omega + i0^+)$. Since the QMC method supplies us only with the imaginary time Green's function $G_{ii}(\tau)$, we used the maximum entropy procedure [27, 28, 29] for providing its analytic continuation. In most cases results from a self-consistent perturbation theory for the Anderson impurity (NCA) [21, 30] were used as a default model for this procedure. This is a nearly ideal combination of methods, since the NCA becomes exact at high frequencies where the QMC data contains little information, and the analytically continued QMC data is essentially exact at low frequencies. A detailed comparison of NCA and QMC results will be presented elsewhere [22]. When a pseudogap was present in the one-particle excitation spectrum, we found that the NCA equations failed to converge due to numerical instabilities. In this limit second-order perturbation theory in U was used to provide a default model for the maximum entropy process.

With either default model, it was extremely important to carefully control both the systematic and especially the statistical errors of the Monte Carlo process. Thus, before analytic continuation, the self consistent process discussed above was allowed to fully converge. Then several runs were per-

formed to obtain a highly accurate average value of Σ . The self-consistency was then turned off, and several runs using this value of Σ were performed to calculate a highly accurate value of $\mathcal{G}(\tau)$ which was then analytically continued.

Results for the half-filled model are shown in Fig. 8. Here $A(\omega)$ is plotted for several values of U when $\beta = 7.2$, $\epsilon = 0$, and $\langle n \rangle = 1$. As the Coulomb

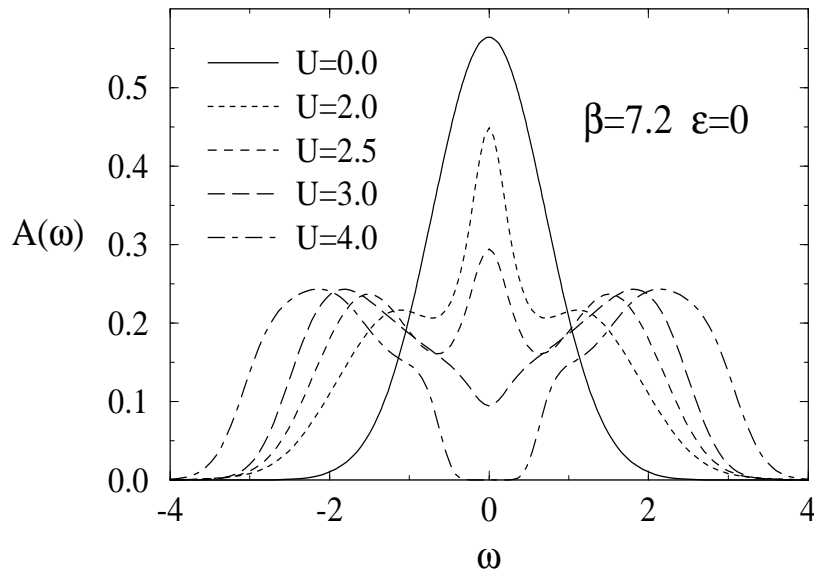


Figure 8: *Evolution of $A(\omega)$ in the paramagnetic phase of the half-filled model.*

repulsion U is increased from zero the broad central peak in the spectrum becomes narrower and is gradually suppressed while at the same time two side bands build up which are carrying the majority of the spectral weight. This kind of behaviour has also been found in different kinds of perturbation

theory [14, 31]. As discussed below, the central peak can be identified with a Kondo-like resonance, and the side peaks as usual with charge transfer on and off the site. As U continues to rise, the spectrum begins to develop a pseudogap at zero frequency when $U > 3.4 \approx U_C$. The “critical” value U_C increases with increasing temperature, and for $U > U_C$ the pseudogap grows linearly in U . This structure is identified as a pseudogap, rather than a gap, since the zero frequency density of states was never identically zero. Rather at $\omega = 0$ it was about 4 orders of magnitude smaller than that of the surrounding features. Indeed, this is consistent with an argument of Krauth and George [32] who argue that in this model the zero frequency density of states is finite for all T , even at $T = 0$.

The evolution of density of states and the filling as a function of ϵ is shown in figure 9. As ϵ is increased from zero, the filling decreases very slowly at first, consistent with the presence of a pseudogap. The filling begins to change rapidly once ϵ is increased to roughly half the gapwidth. The change in filling is enhanced by the presence of a narrow resonance near zero frequency which replaces the pseudogap as soon as the model is doped away from half filling. However, there is a vestige of the Mott pseudogap at higher frequencies.

Perhaps even more interesting is the temperature dependence of the DOS. In Fig. 10 the DOS for $U = 4$ close to half filling ($n \approx 0.94$) is displayed for some typical values of T . While the peaks related to charge excitations are nearly temperature independent, the resonance at the chemical potential is

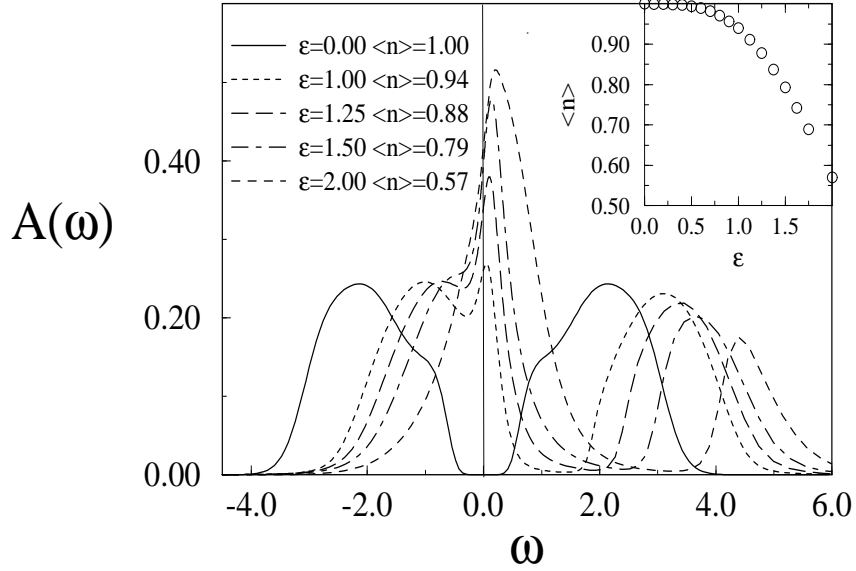


Figure 9: *Evolution of $A(\omega)$ as a function of filling when $\beta = 7.2$ and $U = 4$. The filling versus ϵ is shown in the inset.*

very sensitive to the temperature and evolves roughly as $\ln(T)$ when going from $\beta = 7.2$ to $\beta = 14.4$. It becomes more pronounced at lower temperatures, and apparently disappears completely once the temperature is raised to about twice the width of this feature. As shown in the inset in Fig. 10, the growth of this resonance is correlated with the reduction of the screened local moment $T\chi_{ii}(T)$. In connection with the fact that eqs. (5)-(9) represent an effective Anderson impurity problem, it is evident that this behaviour must be interpreted as a Kondo-like screening of the local moment and consequently the resonance at the Fermi surface can be identified with the Abrikosov-Suhl

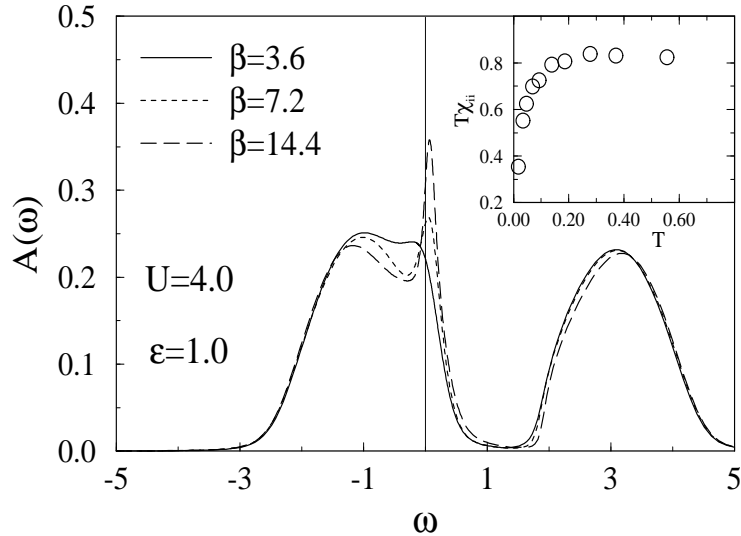


Figure 10: *Evolution of the Kondo-like feature with T . As shown in the inset, the growth of the resonance is correlated with the reduction of the screened local moment $T\chi_{ii}$.*

resonance known to accompany the former. With the reasonable assumption $\Sigma(i0^+) \rightarrow 0$ as $T \rightarrow 0$, we expect $A(0) \rightarrow 1/\sqrt{\pi}$ [33]. Using as the “Kondo”-scale the temperature, where $A(0; T_K) = \frac{1}{2}A(0, T \rightarrow 0)$, we find $T_K \approx t^*/8$ in this case.

Since this Kondo-like feature is pronounced, and occurs right near the Fermi surface, one would expect it to have a strong effect upon a number of properties of the system like resistivity and specific heat [22]. One simple way to obtain an idea how large this influence may be is to inspect the effective mass of the quasiparticles in the system. In Fig. 11, the mass enhancement

factor

$$a^{-1}(T) = 1 - (\text{Im}\Sigma(i\omega_0)) / \omega_0 \quad (15)$$

is plotted versus temperature when $U = 4$ for some typical values of ϵ . Here,

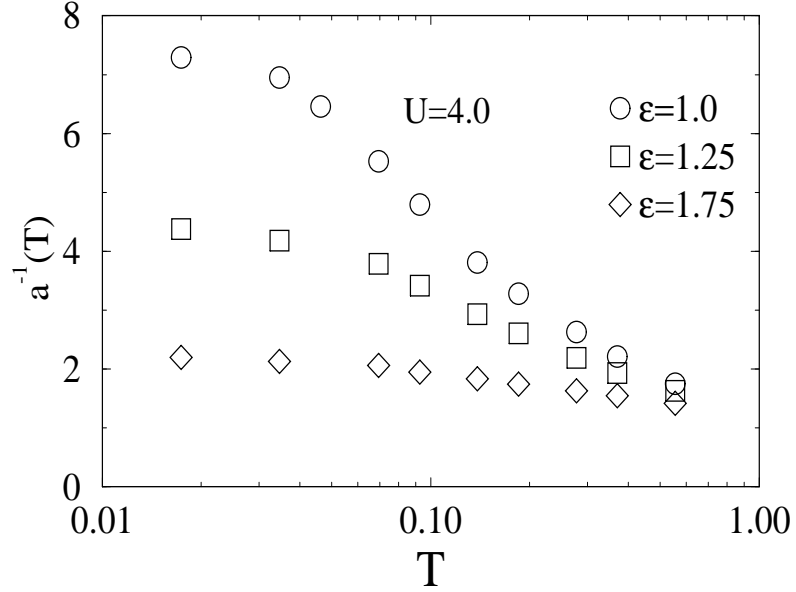


Figure 11: *Mass enhancement $a^{-1}(T) = 1 - (\text{Im}\Sigma(i\omega_0)) / \omega_0$ versus temperature.*

$i\omega_0$ is the lowest Matsubara frequency, and the wave function renormalization factor is given by the zero temperature limit of $a(T)$. As shown in the figure, the mass enhancement factor increases like $\ln(T)$ until the temperature falls well below the Kondo-scale, in which case it saturates. The behaviour $a^{-1}(T) \sim \ln(T)$ has been identified [34] as one of the signatures of marginal Fermi liquid behaviour which has been suggested as a possible

phenomenological picture for the two-dimensional limit of the model (1) [35]. However, it is clear that the infinite-dimensional model close to half filling is not marginal, since a^{-1} saturates to a finite value at low temperatures, corresponding to a usual Fermi liquid with an enhanced effective mass, which is strongly dependent upon filling. In the case when $\epsilon = 1.0$, the filling is roughly $\langle n \rangle \approx 0.94$, and $a^{-1}(0) \approx 7.5$, corresponding to a mass enhancement of $m^*/m \approx 7.5 \approx T_K^{-1}$. Far away from half-filling, it is about one, and as half filling is approached it increases dramatically.

5 Conclusion and Interpretation

The method described in this paper has reduced the infinite dimensional Hubbard model to a self-consistently embedded Anderson impurity problem. Thus for large U the qualitative features of the density of states have an obvious interpretation in terms of the Anderson model spectrum. The upper and lower peaks found correspond to charge transfer on and off the local site. In addition a small resonance at or near the chemical potential occurs which to our opinion must be interpreted in terms of an Abrikosov-Suhl resonance accompanying the screening of the local moment as observed in $T\chi_{ii}(T)$. As well known from the physics of the Kondo effect, this formation of a bound state causes a significant mass enhancement for the quasiparticles in the system as $T \rightarrow 0$.

From the data presented here, it is possible to obtain a very good representation of the phase diagram of the infinite dimensional Hubbard model. For example, the phase diagram for half-filling is illustrated in Fig. 12. At

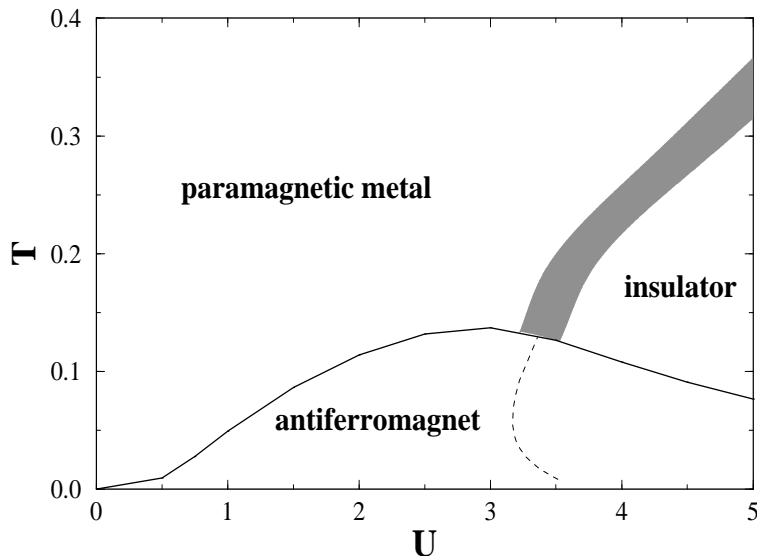


Figure 12: *Phase diagram for the Hubbard model in $d = \infty$ at half filling. The shaded region is centered upon the location of the continuous metal-insulator transition. The extension of this boundary into the antiferromagnetic region is represented by the dashed line.*

temperatures above T_N we find a paramagnetic Fermi liquid state with more or less enhanced quasiparticle masses. This evolves gradually into a Mott-Hubbard phase which is stable beyond some critical value of U . This “insulator” phase is identified with the occurrence of an exponentially small density

of states at zero frequency and is quickly suppressed upon increase of T , because it can only be stabilised when the charge excitation peaks are well separated on the scale of variation of Fermi's function. Since the zero frequency density of states is always finite, no real phase transition (i.e. one with an identifiable order parameter) from the metal to the insulator has occurred. However, when the zero-frequency density of states becomes exponentially small, the dynamic and transport properties [22] of the system change radically in a manner consistent with the change from a metal to an insulator. At low temperatures the system is always antiferromagnetically ordered with a symmetry-induced gap in the one-particle DOS. Upon doping (not shown), the Mott insulator phase vanishes, and the AF region shrinks.

If we artificially extend the metal-insulator boundary into the antiferromagnetic region (the dashed line in Fig. 12), then we find an interesting reentrance: the critical U_c increases with decreasing temperature. This reentrance is not relevant to the present unfrustrated model due to the antiferromagnetism; however, it is relevant to models with sufficient lattice frustration so that the antiferromagnetic transition is suppressed. Such is the case if we include a hopping term to the second next neighbor along each of the coordinate axes equal to the nearest neighbor hopping t . In fact, with this modification, the unperturbed density of states in the $d = \infty$ limit remains Gaussian, with a renormalized energy scale [33]. Our present calculation is relevant to such a model. In our opinion this reentrance must be attributed

to a competition between the Kondo-effect, which never completely vanishes due to the finite DOS at the chemical potential, and the Mott-Hubbard phase. Actually, from inspection of the ground state energy we find that the Abrikosov-Suhl resonance is always favoured when $T \rightarrow 0$ and U large. We emphasize that this behaviour is strongly related to the fact that for $d = \infty$ one always must have $A(0) > 0$, which leads to a small Kondo-effect that eventually kills the Mott-Hubbard transition as $T \rightarrow 0$. Without symmetry breaking due to a magnetic phase transition we expect a similar situation in finite dimensions and $T > 0$ [14]. However, a smaller value of U_c as $T \rightarrow 0$ must be anticipated in this case, because $A(0)$ should decrease exponentially with temperature for sufficient large U .

In conclusion, we have presented a set of self-consistent equations for the Hubbard model which allows one to calculate the properties of strongly correlated systems in the limit of infinite dimensions. Using a quantum Monte Carlo procedure to solve these equations we have shown that the model displays the expected antiferromagnetism when half-filled, and that the single-particle density of states displays a correlation pseudogap. The importance of this result is that it allows an essentially exact solution of the $d = \infty$ Hubbard model in the thermodynamic limit. Thus, solutions now exist for the model in two limits, $d = 1$ and $d = \infty$. With respect to the various phenomenological models it is surely noteworthy that the feature found at the Fermi level provides to some extent a natural way to obtain

unusual properties. Finally, while this method is discussed in the context of the Hubbard model, it could be applied to other strongly correlated models (i.e. the periodic Anderson model) just by changing the form of the undressed Green's functions in (5)-(9). Work on this problem is in progress.

We would like to acknowledge useful conversations with D.L. Cox, N. Grewe, V. Janiš, H. R. Krishnamurthy, M. Ma, A. Millis, A. Olés, R. Scalettar, and Mathew Steiner. One of us (TP) would also like to thank for the hospitality and motivating atmosphere at the physics department of the Ohio State University. This work was supported by the National Science Foundation grant number DMR-9107563, by the National Science Foundation grant number DMR-88357341, the Ohio State University center of materials research and by the Ohio Supercomputing Center.

References

- [1] J. Hubbard, Proc. R. Soc. a**276**, 238(1963); M.C. Gutzwiller, Phys. Rev. Lett. **10**, 159(1963); J. Kanamori, Prog. Theor. Phys. **30**, 257(1963).
- [2] Proceedings of the international conference on “Itinerant-Electron Magnetism”. Physica B+C**91** (1977); for a review about the theory of the Hubbard model see also D. Vollhardt, Rev. Mod. Phys. **56**, 99(1984).
- [3] E.H. Lieb and F.Y. Wu, Phys. Rev. Lett. **20**, 1445 (1968); H. Frahm and V.E. Korepin, Phys. Rev. B**42**, 10533(1990); N. Kawakami and S.-K. Yang, Phys. Rev. Lett. **65**, 2309(1990).
- [4] P.W. Anderson, Phys. Rev. Lett. **64**, 1839(1990); **65** 2306(1990).
- [5] H.J. Schulz, *Proceedings of the Adriatico Research Conference on Strongly Correlated Electron Systems II*, edited by G. Baskaran, A.E. Ruckenstein, E. Tosatti and Yu Lu (World Scientific, Singapore, 1991).
- [6] P.W. Anderson, Phys. Rev. Lett. **67**, 3844(1991).
- [7] W. Metzner and D Vollhardt, Phys. Rev. Lett. **62**, 324 (1989).
- [8] E. Müller-Hartmann, Z. Phys. B **76**, 211 (1989).
- [9] P.G.J. van Dongen and D. Vollhardt, Phys. Rev. Lett. **65**, 1663 (1990).

- [10] M. Jarrell, preprint Nov. 1991. See also the subsequent work of Rosenberg, Zhang, and Kotliar, preprint Feb. 1992 and Georges and Krauth Preprint, Feb. 1992.
- [11] H. Schweitzer and G. Czycholl, *Z. Phys. B* **77**, 327 (1990).
- [12] V. Zlatić and B. Horvatić, preprint.
- [13] B. Menge and E. Müller-Hartmann, *Z. Phys. B* **82**, 237 (1991).
- [14] Th. Pruschke, *Z. Phys. B* **81**, 319(1990).
- [15] V. Zlatić and B. Horvatić, *Phys. Rev.* **B28**, 6904(1983); K. Yamada and K. Yosida, *Theory of Heavy Fermions and Valence Fluctuations*, T. Kasuya and T. Saso, editors (Springer, 1985).
- [16] U. Brandt and Ch. Mielsch, *Z. Phys.* **B75**, 365(1989); **79**, 295(1990).
- [17] V. Janiš and D. Vollhardt, submitted to *Int. J. Mod. Phys. B*.
- [18] The undressed Green's function occurring in the perturbation expansion of the Anderson model is the local component of the solution of the corresponding resonant level model, i.e. where $U = 0$. This has the general form $(G_l(z))^{-1} = z - \epsilon_l + \Delta(z)$.
- [19] J.E. Hirsch and R.M. Fye, *Phys. Rev. Lett.* **56**, 2521 (1986).

- [20] A similar self-consistent QMC procedure was used to treat magnetic impurities in a superconducting host. M. Jarrell, D.S. Sivia, and B. Patton, Phys. Rev. B, **42**, 4804.
- [21] Th. Pruschke and N. Grewe, Z. Phys. B **74**, 439(1989).
- [22] Th. Pruschke and M. Jarrell, to be published.
- [23] W. Langer, M. Plischke and D. Mattis, Phys. Rev. Lett. **23**, 1448 (1969).
- [24] P.G.J. van Dongen, Phys. Rev. Lett. **67**, 757 (1991).
- [25] R.T. Scalettar, D.J. Scalapino, R.L. Sugar and D. Toussaint, Phys. Rev. **B39**, 4711(1989).
- [26] Actually, from the mean-field like nature of the solution in $d = \infty$ one would expect the $d = 3$ data rather to be smaller. This should hold, however, only if we calculated our results with a free DOS as it occurs in a three dimensional system instead of the Gaussian (2) used here.
- [27] J.E. Gubernatis et al., Phys. Rev. B **44**, 6011 (1991).
- [28] R.K. Bryan, Eur. Biophys. J. **18**,165 (1990)
- [29] R.N. Silver et al., Phys. Rev. B, **41**, 2380 (1989).
- [30] N.E. Bickers, D.L. Cox and J.W. Wilkins, Phys. Rev. **B36**, 2036(1987).
- [31] A. Georges and G. Kotliar, Phys. Rev. **B45**, 6479(1992).

- [32] W. Krauth Private Communication, see also [31].
- [33] E. Müller-Hartmann, Z. Phys. **B76**, 216(1989).
- [34] J.W. Serene and D.W. Hess, Phys. Rev. **B44**, 3391(1991).
- [35] C.M. Varma, P.B. Littlewood, S. Schmitt-Rink, E. Abrahams and A.E. Ruckenstein, Phys. Rev. Lett. **63**, 1996(1989).